Mutual Impedance Probe in Collisionless Unmagnetized Plasmas With Suprathermal Electrons—Application to BepiColombo

Nicolas Gilet[1]*, Pierre Henri[1], Gaëtan Wattieaux[2], Minna Myllys[1], Orélien Randriamboarison[1], Christian Béghin[1] and Jean-Louis Rauch[1]

[1] LPC2E, CNRS, Université d'Orléans, Orléans, France, [2] Université de Toulouse, LAPLACE-UMR 5213, Toulouse, France

Context: Mutual impedance experiments are active electric probes providing *in-situ* space plasma measurements. Such active experiments consist of a set of electric antennas used as transmitter(s) and receivers(s) through which various dielectric properties of the plasma can be probed, giving therefore access to key plasma parameters such as, for instance, the electron density or the electron temperature. Since the beginning of the space exploration, such active probes have been launched and operated in Earth's ionospheric and magnetospheric plasmas. More recently and in the coming years, mutual impedance probes have been and will be operated onboard exploratory planetary missions, such as Rosetta, BepiColombo and JUICE, to probe the cometary plasma of 67P/Churyumov-Gerasimenko, the Hermean and the Jovian magnetospheres, respectively.

Aims: Some analytic modeling is necessary to calibrate and analyse mutual impedance observations in order to access to macroscopic bulk plasma quantities. *In situ* particle observations from various space missions have confirmed that space plasmas are out of local thermodynamic equilibrium. This means that particle velocity distributions can be far from a Maxwellian distribution, exhibiting for instance temperature anisotropies, beams or a suprathermal population. The goal of this paper is to characterize the effect of suprathermal electrons on the instrumental response in order to assess the robustness of plasma diagnostics based on mutual impedance measurements in plasmas characterized by a significant amount of suprathermal particles.

Methods: The instrumental response directly depends on the electron velocity distribution function (evdf). In this work, we choose to model suprathermal electrons by considering different approaches using: (i) a kappa evdf, (ii) a double-Maxwellian evdf or (iii) a mix of a Maxwellian evdf and a kappa evdf. For each case, we compute the spatial distribution of the electrostatic potential induced by the transmitters, discretized and modeled here as an ensemble of pulsating point charges.

Results: We apply our modeling by building synthetic mutual impedance spectra of the PWI/AM^{2}P probe, lauched in October 2018 onboard the Mercury Magnetospheric Orbiter (MIO/MMO) spacecraft of the BepiColombo exploratory space mission, in order to calibrate and analyse the future electron observations in the plasma environment of Mercury.

1. INTRODUCTION

Mutual impedance experiments are active electric experiments designed to measure *in-situ* space plasma bulk properties such as the electron density and the electron temperature (Chasseriaux et al., 1972). The measurement is usually based on the electric coupling between pairs of electric dipole antennas embedded in the plasma to be probed (Storey et al., 1969). The transmitting electrodes inject an oscillating current at a given frequency in the surrounding plasma. This current and the electric potential difference induced on the receiving antenna are both measured simultaneously at the same frequency. A mutual impedance spectrum is built by varying, step by step, the emitted frequency.

Initially developed in geophysical fields prospecting to measure the resistivity of the ground (Wenner, 1915; Schlumberger, 1920; Storey et al., 1969), mutual impedance experiments have been used on Earth ionospheric and magnetospheric missions (Beghin and Debrie, 1972; Décréau et al., 1978; Beghin et al., 1982). More recently, mutual impedance experiments have been used to probe interplanetary plasmas. The Mutual Impedance Probe (MIP), as a part of the Rosetta Plasma Consortium (RPC), on board the Rosetta orbiter (Trotignon et al., 2007), measured the electron density in the ionosphere of the comet 67P/Churuymov-Gerasimenko (Henri et al., 2017). The Active Measurement of Mercury's Plasma (AM^{2}P) instrument (Trotignon et al., 2006) from the Plasma Wave Investigation (PWI) is currently onboard the Mercury Magnetospheric Orbiter (MIO/MMO) of the BepiColombo mission successfully launched in October 2018. After the 7.2 years cruise phase, this experiment will constrain the plasma bulk properties in the Hermean magnetosphere. Two others experiments from the PWI consortium will operate in the Hermean magnetosphere and in the solar wind close to Mercury in order to measure the electron density onboard the MIO/MMO spacecraft. First, a thermal electrostatic noise spectroscopy experiment (PWI/SORBET, Moncuquet et al., 2006) will operate using the WPS antenna (Benkhoff et al., 2010; Kasaba et al., 2010). This experiment makes use of passive measurements combined to the Quasi-Thermal Noise spectroscopy technic to access the plasma bulk properties such as the electron density or the electron temperature through a diagnostic of the voltage power spectrum (Meyer-Vernet et al., 2017). Second, the spherical probes located at the end of the two MEFISTO antennas will be operated using the Langmuir Probe measurement technique to also access the plasma bulk properties (Blomberg et al., 2006). A strong advantage of the MIO/MMO

spacecraft of BepiColombo is that it is the first time a single spacecraft will carry these three experiments that will be operated simultaneously to provide bulk plasma measurements, thus enabling to take advantage of the strength of each measurement technic and going beyond the intrinsic limitations of each. In the future, the Mutual Impedance MEasurement (MIME) as a part of the Radio Wave Plasma Investigation (RPWI) is being developed for the Jupiter ICy Moons Explorer (JUICE) mission to constrain the Jovian magnetospheric plasma and the ionosphere of Ganymede.

The mutual impedance between two electric antennas immersed in a plasma strongly depends on the plasma properties, in particular the electron velocity distribution function (evdf). As mutual impedance experiments have been used in several plasma environments, many theoretical works have been carried out (Grard, 1969; Navet et al., 1971; Rooy et al., 1972; Pottelette et al., 1975; Beghin, 1995) to characterize the properties of mutual impedance experimental behavior from cold (modeled by a Dirac evdf) to hot (modeled by a Cauchy or Maxwellian evdf) plasmas. However, the impact of high-energy electron called suprathermal electrons, omnipresent in space plasmas, had not been sufficiently considered in the past. The goal of this paper is therefore to fill this gap and study the effect of suprathermal electrons on the instrumental response of mutual impedance experiments.

Indeed, suprathermal electrons are ubiquitous in collisionless space plasmas: in the solar wind (Vasyliunas, 1968), in the Hermean magnetosphere (Christon, 1987; Ho et al., 2016), in the magnetosphere of Saturn (Schippers et al., 2008) or in the ionosphere of the comet 67P/Churyumov-Gerasimenko (Clark et al., 2015; Broiles et al., 2016; Myllys et al., private communication). The evdf in the presence of a suprathermal tail is usually described as the sum of thermal (core) and a non-thermal (halo) parts (Maksimovic et al., 2005):

$$f = f_{core} + f_{halo} \qquad (1)$$

where the thermal part is usually described by a Maxwellian evdf and the non-thermal part by a kappa evdf (Lazar et al., 2017). The kappa evdf can be seen as a generalization of the Maxwellian evdf, nearly Maxwellian at low energies and decreases as a power-law at higher energies (Summers and Thorne, 1991). In the literature, observed electron distribution functions have also been modeled by other evdf or combinations of evdf: Maksimovic et al. (1997) fitted the evdf observed by Ulysses in the solar wind with a single kappa evdf, while Schippers et al. (2008), Broiles et al. (2016) and Myllys et al. (submitted) used two kappa evdf to fit the

observed evdf respectively in the Saturn magnetosphere and in the ionosphere of 67P/Churyumov-Gerasimenko.

Previous works investigated the instrumental response of mutual impedance experiments in a presence of suprathermal particles but only in restrictive cases: (i) in a plasma described by monoenergetic evdf [Dirac delta evdf, Grard (1997)] or (ii) in a plasma described by a sum of two Maxwellian evdf on a restricted hot-to-cold electron density and in the limit where the Debye length λ_D is very small compared to the distance between the transmitter and the receiver antennas (Pottelette and Storey, 1981). Recently, Gilet et al. (2017) developed a model of the electrostatic radiated potential in a plasma described by a sum of two Maxwellian evdf down to conditions encountered in interplanetary and planetary plasmas (i.e., $\lambda_D \sim$ transmitter-receiver distance). In this present work, we consider suprathermal electrons associated to a collisionless plasma, for which the hypothesis of thermodynamic equilibrium is no longer valid. In other words, this means that suprathermal particles cannot be considered as a Maxwellian distribution. Instead, we will make use of kappa distributions to model out-of-thermodynamic equilibrium evdf for suprathermal electrons. Especially, we study the robustness of the plasma density measurement through the mutual impedance method in the presence of energetic electrons. This new model is applied to the mutual impedance experiment PWI/AM^{2}P onboard the Mercury Magnetospheric Orbiter (MIO/MMO) of the BepiColombo mission (Trotignon et al., 2006; Benkhoff et al., 2010) to prepare the future calibration of the experiment.

This paper is organized as follows: in section 2, we remind the definition of the electric potential induced by a pulsating point charge in a plasma, when evdf is a combination of kappa and Maxwellian evdf. As mutual impedance experiments are based on the propagation of an electric field in a plasma, we also remind the dispersion relations of the linear eigenmodes of interest of such experiments in section 3. This is done for each considered evdf and it allows to better understand, at least qualitatively, the damping rate of the radiated electric potential in the frequency range encompassing the electron plasma frequency. The electric potentials are then computed and compared to the results obtained from the different evdf such as those are considered in this work. We apply the developed computation to the active quadrupolar mutual impedance probe PWI/AM^{2}P onboard the MIO/MMO spacecraft in section 4. We show that in certain limit (high electron density, small Debye length), the presence of the suprathermal electrons do not change the instrumental response. However, for small enough electron density and large enough Debye length, the more suprathermal electrons are presents, the easier the electron plasma frequency can be measured. This seemingly counterintuitive result is due to the fact that the Debye length is smaller for kappa evdf at equivalent (Maxwellian) temperature. In section 5, we compute the AM^{2}P spectra in typical solar wind plasma and in Hermean magnetospheric plasma, using respectively modeling of evdf from several solar space missions (Pierrard et al., 2016) and the *in-situ* particles measurement from a Mercury flyby by Mariner 10 (Baker et al., 1986). We show how the measurement of the plasma density is not influenced by suprathermal electrons

in typical solar wind plasma close to the Mercury perihelion (0.31 AU) but can be slightly affected close to the aphelion (0.47 AU). Moreover, we show that the detection of the plasma frequency might be challenging in the low density Hermean magnetospheric plasma. Finally we conclude our study in section 6.

2. MODEL

The electric potentiel ϕ induced in an isotropic, homogeneous plasma by a pulsating point charge $Q.exp(i\omega t)$, at frequency ω, at a radial distance r from the charge Q is given by:

$$\phi(\omega, r) = \frac{Q}{4\pi \varepsilon_0} \frac{2}{\pi} \lim_{Im(\omega) \to 0} \int_0^{+\infty} \frac{\sin(kr)}{kr} \frac{dk}{\varepsilon_l(k, \omega)} \quad (2)$$

where ε_l is the longitudinal dielectric function of the plasma, k is the wavelength and ε_0 is the vacuum permittivity.

We recall the longitudinal dielectric function ε_l for electrostatic waves in an unmagnetized plasma (Krall and Trivelpiece, 1973):

$$\varepsilon_l(k, \omega) = 1 + \frac{\omega_{pe}^2}{k^2} \int \frac{k.\nabla_v f_0}{\omega - k.v} dv \quad (3)$$

with f_0 the evdf at equilibrium state, v the electron velocity and ω_{pe} the electron plasma frequency defined by $\omega_{pe} = (n_e e^2 / m_e \varepsilon_0)^{1/2}$ where n_e is the electron density, e the electric charge, m_e the electron mass and ε_0 the vacuum permittivity.

The longitudinal dielectric function directly depends on the electron velocity distribution function. The evdf typically observed in the solar wind and in magnetospheres can be described as a sum of different evdf as follows (Maksimovic et al., 2005):

$$f_0 = f_{core} + f_{halo} \quad (4)$$

with f_{core} the velocity distribution function of the core electrons, that can be seen as the thermal component, f_{halo} the velocity distribution function of the halo electrons, that can be seen as the suprathermal component. In this work, we have not taken into account other suprathermal electron contributions such as the solar wind strahl (Štverák et al., 2009). While state-of-the-art models of mutual impedance experiments do not enable to model components of the distribution functions that are not symmetric in velocity space (such as the strahl), we later argue and justify that the strahl contribution to the modeling of mutual impedance spectra can be neglected, at least in the limit of the solar wind parameters range close to the perihelion (section 5).

In the literature, f_{core} is usually modeled by a Maxwellian evdf and f_{halo} by a kappa evdf (Lazar et al., 2017). In some cases, f_0 can be directly treated as a single kappa evdf to model both core and halo electrons in a single description on the solar wind for instance (Maksimovic et al., 1997), or in more complex situations as a sum of two kappa evdf as in the magnetosphere of Saturn (Baluku et al., 2011) or in the ionosphere of the comet 67P/Churyumov-Gerasimenko (Clark et al., 2015; Broiles et al., 2016; Myllys et al., private communication).

We use the following notations for a Maxwellian evdf f_{Maxw} and a kappa evdf f_κ:

$$f_{Maxw}(v) = \frac{1}{\pi^{3/2} v_{th}^3} e^{-v^2/2v_{th}^2} \tag{5}$$

$$f_\kappa(v) = (\pi \kappa \theta^2)^{-3/2} \frac{\Gamma(\kappa+1)}{\Gamma(\kappa-1/2)} \left(1 + \frac{v^2}{\kappa \theta^2}\right)^{-(\kappa+1)} \tag{6}$$

where $v_{th} = (k_B T_e/m_e)^{1/2}$ is the electron thermal velocity associated to the electron temperature T_e, k_B the Boltzmann constant, Γ the classical gamma function, $\theta = [(2\kappa-3)/\kappa]^{1/2} v_{th}$ the generalized thermal speed, with κ is a real number and $\kappa > 3/2$. We remind the reader that the kappa evdf is a generalization of the Maxwellian evdf for $\kappa \to +\infty$.

In this study, we choose to normalize distances to the Debye length of the Maxwellian evdf $\lambda_{D,Maxw} = (k_B T_e/m_e \omega_{pe}^2)^{1/2}$. As pointed out by Chateau and Meyer-Vernet (1991), the comparison between a Maxwellian and a kappa evdf only makes sense in plasmas characterized by the same density and temperature. In that case, the corresponding Debye length for a kappa evdf is defined as follows:

$$\lambda_{D,\kappa} = \sqrt{\frac{2\kappa-3}{2\kappa-1}} \lambda_{D,Maxw} \tag{7}$$

For a collisionless isotropic plasma with a combination of n_M Maxwellian and n_κ kappa evdf, the longitudinal dielectric function ε_l reads (Mace et al., 1999):

$$\varepsilon_l(K, \Omega) = 1 - \sum_{i=1}^{n_M} \frac{Y_i^2}{\Omega_i^2} Z'(Y_i) - \sum_{j=1}^{n_\kappa} \frac{(\kappa_j-1)^2}{(\kappa_j-3/2)^2} \frac{Y_j^2}{\Omega_j^2} Z'_{\kappa_j-1}$$
$$\left[\left(\frac{\kappa_j-1}{\kappa_j-3/2}\right)^{1/2} Y_j\right] \tag{8}$$

where:

$$K = k\lambda_{D,ref} \tag{9}$$

$$\Omega = \frac{\omega}{\omega_{pe}} \tag{10}$$

$$\Omega_i = \frac{\omega}{\omega_{pe,i}} \tag{11}$$

$$Y_i = \frac{\Omega_i}{\sqrt{2\mu_i/\tau_i} K} \tag{12}$$

where $\lambda_{D,ref}$ is the Debye length of the hottest electron population. As explained above, if the kappa population is the hottest population, $\lambda_{D,ref}$ is normalized to the corresponding $\lambda_{D,Maxw}$. In addition, we define μ_i (resp. τ_i) the density (resp. temperature) ratio between the hottest population and the i-th population and i.e., $\mu_i = n_{hot}/n_i$ and $\tau_i = T_{hot}/T_i$. Z' and Z'_{κ_j-1} are, respectively, the first derivative of the plasma dispersion function Z (Fried and Conte, 1961) and of the

modified plasma dispersion function Z_κ (Summers and Thorne, 1991). The modified plasma dispersion function Z_κ reads:

$$Z_\kappa(\xi) = \frac{i(\kappa+\frac{1}{2})(\kappa-\frac{1}{2})}{\kappa^{3/2}(\kappa+1)} {}_2F_1[1, 2\kappa+2; \kappa+2; \tfrac{1}{2}(1 - \xi/i\sqrt{\kappa})] \tag{13}$$

where ${}_2F_1$ is the Gauss hypergeometric function. The main properties of Z and Z_κ can be found in Fried and Conte (1961) and Mace and Hellberg (1995), respectively[1]. Using the chosen normalization, Equation (2) that gives the electrostatic potential transmitted in a plasma distance $R = r/\lambda_{D,ref}$ by a pulsating point charge at frequency Ω rewrites (Gilet et al., 2017):

$$\frac{\phi}{\phi_0}(\Omega, R) = \frac{2R}{\pi} \lim_{Im(\Omega)\to 0} \int_0^\infty \frac{sin(KR)}{KR} \frac{1}{\varepsilon_l(K,\Omega)} dK \tag{14}$$

The computation of this radiated electrostatic potential has been carried out using the numerical method described in Gilet et al. (2017) and generalized to a sum of different evdf following Equation (8).

3. ELECTRIC POTENTIAL RADIATED IN A PLASMA WITH SUPRATHERMAL ELECTRONS

In this section, we discuss the radial profile of the electric potential defined in section 2 (Equation 14) for the following electron velocity distribution functions: a kappa evdf (section 3.2) and a sum of a core Maxwellian and a halo kappa evdf (section 3.3). The propagation of the electric potential in the plasma is strongly constrained by the different available linear eigenmodes. We introduce these modes in section 3.1.

3.1. Linear Eigenmodes

We remind the analytic approximation of the linear eigenmodes of the plasma characterized by the different evdf considered in this work (solutions of the dispersion relation $\varepsilon_l(K, \Omega) = 0$) of direct interest in the presence of suprathermal electrons. These modes determine the resonances that shape the mutual impedance spectra. While the longitudinal dielectric function corresponding to a Maxwellian or a kappa evdf has infinite eigenmodes, the least damped modes are the one that contribute most to model the propagation of the electric potential in a plasma. In particular, for a single evdf, the least damped pole, corresponding to Langmuir waves, gives the main contribution to the propagation of the radiated potential in a single electron population plasma, such as a Maxwellian evdf (Chasseriaux et al., 1972; Beghin, 1995). In the large phase velocity limit $\omega/k \gg v_{th}$, with a Maxwellian evdf, the dispersion relation of the Langmuir waves are the following (Krall and Trivelpiece, 1973):

$$\omega_{L,Maxw}(k) = \omega_{pe}\sqrt{1 + 3(k\lambda_D)^2} - i\sqrt{\frac{\pi}{8}} \frac{\omega_{pe}}{(k\lambda_D)^3} e^{-\frac{1}{2(k\lambda_D)^2} - \frac{3}{2}} \tag{15}$$

---

[1]For practical use, we remind that the plasma dispersion function satisfies the differential equation $Z'(y) = -2(1 + yZ(y))$ and derived from the Faddeeva function (or the scaled complex complementary error function): $Z(y) = i\sqrt{\pi}w(y)$

For a single kappa evdf, the Langmuir waves are characterized in the limit $\omega/k \gg \theta$ by the dispersion relation (Mace and Hellberg, 1995):

$$\omega_{L,\kappa}(k) = \omega_{pe}\sqrt{1 + 3(k\lambda_D)^2} - i\pi^{1/2}\frac{\Gamma(\kappa+1)}{\Gamma(\kappa-1/2)}\omega_{pe}(2\kappa-3)^{\kappa-1/2}$$
$$(k^2\lambda_{D,\kappa}^2)^{\kappa-1/2} \tag{16}$$

The real frequency (oscillating part) from these dispersion relations are similar, while the damping rate is strongly different and depends on the κ-value. Note that, hereafter, the radiated potentials expressed in a plasma characterized be a Maxwellian or a kappa distribution will be compared for plasmas characterized by the same electron density and temperature. Thus, at equivalent temperature, the Debye length of the kappa evdf is expressed as in Equation (7), so that it is actually smaller than the corresponding Maxwellian Debye length. Note that these analytical expressions are computed within strong approximations (long wavelength limit for instance) that are usually not relevant for the instrumental modeling, as the transmitter-receiver distance can be as small as a few Debye lengths. To go beyond these analytical, though useful, approximations, we also compute numerically the dispersion relations.

Figure 1 (left panel) shows the dispersion relation of the Langmuir pole for a Maxwellian evdf and for different κ-values (from $\kappa = 2$ to 24). From a practical point of view, the position of the Langmuir pole on the real K-space is estimated from the position of the maximum of $Im(1/\varepsilon_l(K,\Omega))$, that is plotted in **Figure 1** (right panel). The position of the Langmuir pole projected in the real K-space is similar between the kappa evdf and the Maxwellian evdf, as expected analytically (see Equations 15 and 16). Regarding the damping rate γ, it can be qualitatively constrained by the shape of $Im(1/\varepsilon_l(K,\Omega))$ close to the projection of the Langmuir pole on the real K-space. Indeed, the flatter the shape of $Im(1/\varepsilon_l(K,\Omega))$, the farther away the pole from the real K-space i.e., the damping rate γ is high.

For a plasma characterized by two different electron populations, such as a sum of two Maxwellian evdf or a mix of a Maxwellian core evdf and a halo kappa evdf, two different modes both strongly contribute to the propagation of the electric potential (Mace et al., 1999; Gilet et al., 2017) namely the (modified) Langmuir mode and the electron acoustic mode. For convenience, we report here only the variation of the real part of the frequency with the wavevector, issued from the

dispersion relations. The damping rate can be found in the hereby mentioned references.

For a plasma modeled by a mix of a Maxwellian core and a halo kappa evdf or by a sum of two Maxwellian evdf (Gilet et al., 2017), in the limit $\omega/k \gg \theta_h \gg \nu_c$, the dispersion relation of the (modified) Langmuir waves is expressed by:

$$\omega_{L2}(k) = \omega_{pe}\sqrt{1 + 3\left(\frac{n_h}{n_{tot}}\right)^2 \left(\sqrt{\frac{2\kappa-3}{2\kappa-1}}k\lambda_{D,Maxw}\right)^2} \tag{17}$$

In the limit of an intermediate phase velocity i.e., $\nu_c \ll \omega/k \ll \theta_h$ the dispersion relation of the electron acoustic mode is given by (Mace et al., 1999; Gilet et al., 2017):

$$\omega_{EAW}(k) = \omega_{p,c}\sqrt{1 + 3k^2\lambda_{D,c}^2 - \frac{1}{\left(\sqrt{\frac{2\kappa-3}{2\kappa-1}}k\lambda_{D,Maxw}\right)^2}} \tag{18}$$

We have also computed the useful function $Im(1/\varepsilon_l(K,\Omega))$ in a two-electron temperature plasma, in a limit where the electron acoustic and the Langmuir modes co-exist (here $n_h/n_c = 1$, $T_h/T_c = 100$). **Figure 2** shows $Im(1/\varepsilon_l(K,\Omega))$ for (i) an evdf modeled by a sum of a Maxwellian core and a kappa halo evdf for different κ-values (κ from 2 to 24) and (ii) an evdf modeled by a sum of two Maxwellian evdf. As expected, $Im(1/\varepsilon_l(K,\Omega))$ has two maxima due to the presence of the electron acoustic and the Langmuir modes. For small κ-values, the first pole is not well visible. Indeed, as explained by Mace et al. (1999), for a fixed halo-to-core temperature ratio, the domain of existence of the electron acoustic mode is reduced for lower κ-values.

3.2. Radiated Potential for a Single Kappa Evdf

In order to characterize the effect of suprathermal electrons on the radiated electrostatic potential, we have computed the potential for two frequencies such that no eigenmode propagates in a first case ($\Omega = 0.75$) and a Langmuir mode propagates without being damped much, in a second case ($\Omega = 1.10$). The radial profile of the electrostatic potential, expressed in terms of distance to the transmitter is shown in **Figure 3** for different kappa values ($\kappa = 2, 7$, and 24) and for a Maxwellian evdf ($\kappa \rightarrow \infty$), with equal temperatures (Equation 7). The distances are shown in logarithmic scales.
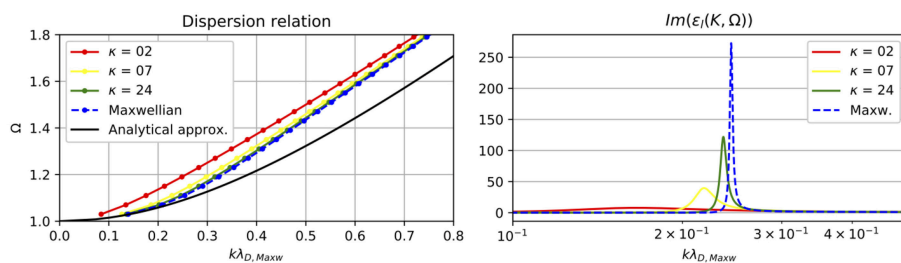
FIGURE 1 | (Left panel) Dispersion relation found by simulation for different κ−values ($\kappa = 2, 7$ and 24) and the Maxwellien evdf ($\kappa \rightarrow +\infty$) with the analytical approximation (black line). **(Right panel)** $Im(1/\varepsilon_l(K,\Omega))$ for the same evdf.
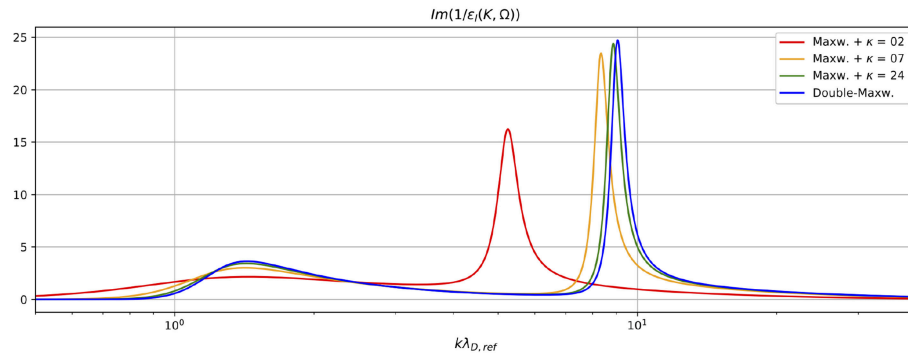
FIGURE 2 | $Im(1/\varepsilon_l(K, \Omega))$ for $\Omega = 1.10$ in a plasma modeled by a mix of a core Maxwellian evdf and a halo kappa evdf for several κ-values ($\kappa = 2, 7, 24$) and a double Maxwellian evdf, where the modified Langmuir mode and the electron acoustic mode co-exists (here: $n_h/n_c = 1$ and $T_h/T_c = 100$). $\lambda_{D,Ref}$ is the Debye length of the halo Maxwellian evdf.
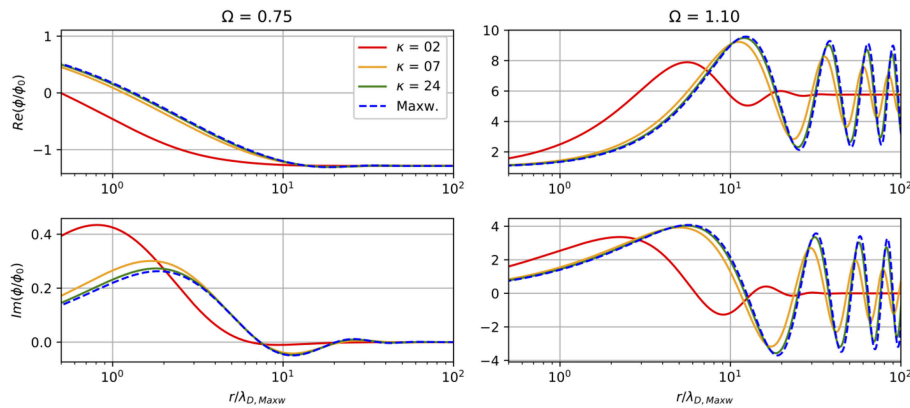
FIGURE 3 | Radiated electrostatic potential for $\Omega = 0.75$ (left column) and $\Omega = 1.10$ (right column) compared to the distance to the transmitter normalized by $\lambda_{D,Maxw}$ in logarithmic scale : the real part (first panel) and the imaginary part (second panel) for different kappa evdf (here $\kappa = 2, 7$ and 24) in colored continuous lines and a Maxwellian evdf ($\kappa \rightarrow +\infty$) in dashed line.

Note that for the two frequencies Ω, the real part of ϕ/ϕ_0 tends to the inverse of the cold plasma dielectric constant $\varepsilon_c = \frac{1}{1-\Omega^{-2}}$ (here $\varepsilon_c^{-1} = -1.29$ for $\Omega = 0.75$ and $\varepsilon_c^{-1} = 5.76$ for $\Omega = 1.10$) and the imaginary part tends to 0, as expected (Beghin, 1995; Gilet et al., 2017).
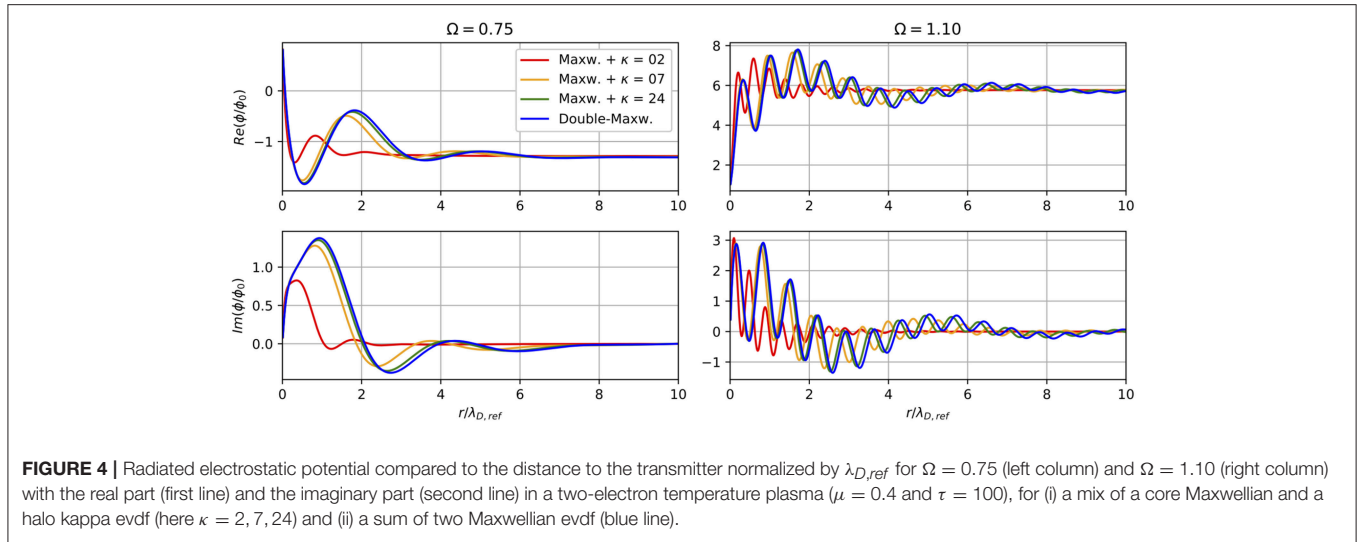
At frequencies higher than the electron plasma frequency, here $\Omega = 1.10$ (right column), the real and the imaginary part of the radiated potential oscillate. The radiated potential in a plasma modeled by a kappa evdf tends to the potential of the Maxwellian evdf when κ increases (here $\kappa > 10$) as expected. However, for the low κ-values, the radiated potential is more damped. This is explained by the higher damping rate γ (section 3.1) for the evdf characterized by the presence of suprathermal electrons. Moreover, the wavelength of the oscillations decreases (from $\sim 25R$ to $\sim 14R$) while the suprathermal electrons contribution increases, as expected from the linear theory of Langmuir waves in a kappa distribution plasma[2].

For frequencies lower than the electron plasma frequency ($\Omega = 0.75$ in **Figure 3**, left panel), the radiated potential does not oscillate because no eigenmode exists at this frequency range. This has a strong implication on the mutual impedance spectrum in particular when the transmitter-receiver distance is short compared to the Debye length that is developed in section 4.

3.3. Radiated Potential for a Mix of Kappa and Maxwellian evdf

We have also investigated the radial variation of the radiated electric potential injected in a plasma modeled with a mix of a core Maxwellian evdf and a halo kappa evdf, as typically observed in the solar wind plasma. In this section, all distances are normalized to the Debye length of the Maxwellian evdf corresponding to the Debye length of the kappa evdf (see Equation 7). The computed potential is illustrated in **Figure 4** in a region where the electron acoustic mode exists (here $n_h/n_c = 0.4$ and $T_h/T_c = 100$) for different κ-values.

---

[2]Note that the wavelength computed from the analytical dispersion relation ($\lambda = 2\pi/K$) is close to the wavelength computed numerically and corresponding to the oscillations of the modeled radiated potential, as expected.

FIGURE 4 | Radiated electrostatic potential compared to the distance to the transmitter normalized by $\lambda_{D,ref}$ for $\Omega = 0.75$ (left column) and $\Omega = 1.10$ (right column) with the real part (first line) and the imaginary part (second line) in a two-electron temperature plasma ($\mu = 0.4$ and $\tau = 100$), for (i) a mix of a core Maxwellian and a halo kappa evdf (here $\kappa = 2, 7, 24$) and (ii) a sum of two Maxwellian evdf (blue line).

First, at frequencies higher than the electron plasma frequency (here $\Omega = 1.10$), the radiated potential is characterized by a superposition of two characteristic waves due to the transmission of both electron and Langmuir fluctuations (section 3.1), as been observed in **Figure 4** (right column). In this case, the Langmuir wavelength is larger than the electron acoustic wavelength. For both oscillations, the waves are more damped when there are more suprathermal electrons in the plasma (i.e., for decreasing κ), as expected from a large Landau damping at small κ.

Second, at frequencies smaller than the electron plasma frequency (here $\Omega = 0.75$), contrary to the potential radiated in a plasma with a single evdf, the potential oscillates due to the electron acoustic mode. The potential is more damped when the suprathermal part increases (i.e., κ-value decreases). Note that this oscillation is strongly damped, though, so that we do not expect the signal propagating further in the plasma. This means that in the case of a receiver located far (in terms of ion acoustic wavelengths) from the transmitter, we do not expect a strong signature in the mutual impedance spectra, while the instrument shall be sensitive to the ion acoustic mode adapted to the transmitter-receiver distance, i.e., we expect the mutual impedance spectra to exhibit the signature of the ion acoustic mode which wavelength is twice the transmitter-receiver distance.

3.4. Mutual Impedance Responses

The potential modeled in the previous section is used to compute the mutual impedance response. Indeed, the transmitters inject an oscillating current $I(\Omega)$ at a given frequency while the receivers measure the (complex) amplitude of the electric potential $V(\Omega)$ at the same frequency. The mutual impedance $Z(\Omega) = \Delta V(\Omega)/I(\Omega)$ is then directly related to the difference between the electric potential $\Delta V(\Omega) = V_{R_2}(\Omega) - V_{R_1}(\Omega)$, radiated by the different emitters at frequency Ω and measured by two receivers R_1 and R_2. To isolate the effect of the plasma to the potential radiated by the emission part of a mutual impedance probe, we work with the mutual impedance spectrum normalized

to the spectrum that is obtained in vacuum

$$H(\Omega) = \frac{Z}{Z_0} = \frac{V_{R_2}(\Omega) - V_{R_1}(\Omega)}{V_{R_2,0} - V_{R_1,0}} \qquad (19)$$

where Z and Z_0 represent the mutual impedance of a probe surrounded by a plasma and by the vacuum, respectively, and V_{R_i} (resp. $V_{R_i,0}$) is the voltage measured by the receiver R_i in the plasma (resp. in vacuum):

$$V_{R_i}(\Omega) = \frac{1}{4\pi\epsilon_0} \sum_{j=1} \frac{\phi}{\phi_0}(\Omega, d_{ij}/\lambda_{D,ref}) \frac{q_j}{d_{ij}} \qquad (20)$$

$$V_{R_i,0} = \frac{1}{4\pi\epsilon_0} \sum_{j=1} \frac{q_j}{d_{ij}} \qquad (21)$$

where q_j is the charge of the jth transmitter and d_{ij} is the distance between the receiver R_i and the jth transmitter, ϕ and ϕ_0 are the electric potential radiated by a pulsating point charge embedded in the plasma or within vacuum, respectively.

The electron plasma frequency is located in the close vicinity of the maximum amplitude of the mutual impedance response (Storey et al., 1969; Chasseriaux et al., 1972). The total electron density, n_{tot}, is then determined from the electron plasma frequency f_{pe} with $n_{tot} = (f_{pe}/8.98)^2$ (n_{tot} is expressed in cm^{-3} and $f_{pe} = \omega_{pe}/2\pi$ in kHz).

4. APPLICATION TO THE BEPICOLOMBO MUTUAL IMPEDANCE PROBE AM²P

In this section, we apply the modeling of the electric potential radiated in a plasma with suprathermal electrons, described previously, to the computation of synthetic mutual impedance spectra. We aim at characterizing the effect of suprathermal electrons on instrumental response of the mutual impedance probe AM²P of the Plasma Wave Investigation (PWI) consortium (Kasaba et al., 2010) onboard the Mercury
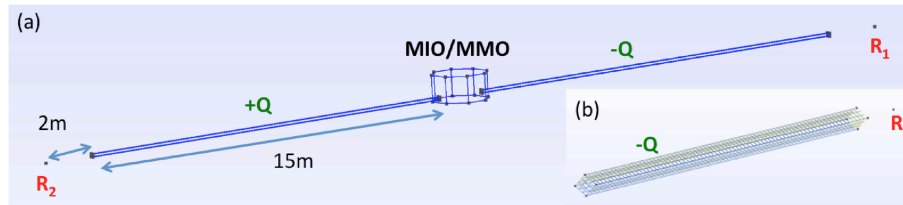
FIGURE 5 | (a) AM^{2}P geometry consists on two 15 m-antennas on both sides of the MMO spacecraft with two receivers, R_1 and R_2, located at 2 m of each end of booms, **(b)** example of the meshing of one AM^{2}P antenna.

Magnetospheric Orbiter (MIO/MMO) of the BepiColombo mission. The PWI/AM^{2}P experiment will measure the plasma bulk properties of the Mercury magnetospheric and Solar wind plasma such as the electron density (in the 0.02 to 180 cm^{-3} range, corresponding to f_{pe} from 0.7 to 120 kHz) and the electron temperature, in a range which depends on plasma conditions (Trotignon et al., 2006). The BepiColombo spacecraft has been launched successfully in October 2018, for an interplanetary cruise phase of 7.2 years (until December 2025) with one Earth flyby, two Venus and six Mercury flybys before the nominal mission science operations performed for one and a half Earth year (about 6 Hermean years) and a planned extension of one Earth year, corresponding to 4 extra Hermean years).

The MIO/MMO spacecraft will have an elliptic polar orbit of 400 × 11,824 km (Benkhoff et al., 2010). From the observations of the MESSENGER mission (Johnson et al., 2012), the interplanetary and Hermean magnetic fields are such that the electron cyclotron frequency is expected to be negligeable compared to the electron plasma frequency for low latitudes or high enough distances from Mercury. The modeling of the electric radiated potential described in this paper is only valid in an unmagnetized plasma, i.e., where the electron-cyclotron frequency f_{ce} is negligible compared to the electron plasma frequency f_{pe}, therefore, we hereafter focus on the AM^{2}P modeling in the solar wind plasma and in the Hermean magnetosphere far from the cusps. Other analysis methods shall be considered (Béghin et al., 2017) or developed in strongly magnetized regions.

4.1. PWI/AM^{2}P Antenna Configuration

The PWI/AM^{2}P quadrupolar probe consists of (i) two transmitting 15m-antennas of 1cm-diameter located on both sides of the MIO/MMO spacecraft and (ii) two receivers located at 2m of the end of the transmitting antennas (**Figure 5**). In this model, the transmitting antennas have been discretized in about thousand rectangular sub-elements, with the center of each sub-element considered as a pulsating point charge, while the receiving antennas are considered as being punctual. This experiments works in the so called Double-Wire (or push-pull) mode for which the pulsating charge on one transmitting antenna is opposite to that of the second transmitting antenna, in other words they are in phase opposition. Given this geometry and charge configuration, the expected mutual impedance is

modeled using Equation (19), combined with Equations (20) and (21).

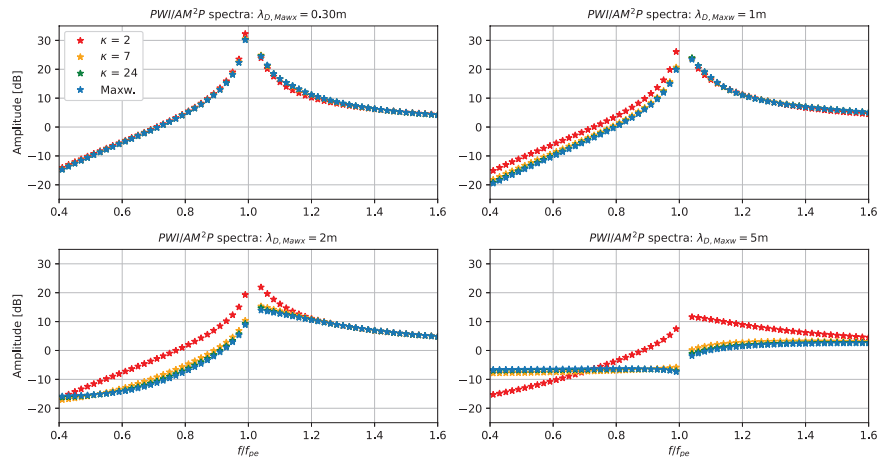## 4.2. Modeling of the AM^{2}P Mutual Impedance Spectra

In the following, the synthetic instrumental response of PWI/AM^{2}P is computed for (i) a single kappa evdf (section 4.2.1) and (ii) a mix of a halo kappa evdf and a core Maxwellian evdf (section 4.2.2). In this section, we consider a large range of plasma parameters in order to characterize the effect of suprathermal electrons in different regimes. We will focus on the plasma conditions in the solar wind and at Mercury expected to be encountered by the MIO/MMO spacecraft in section 5.

4.2.1. AM^{2}P Spectra With a Single Kappa evdf

We have modeled the PWI/AM^{2}P mutual impedance response for different κ-values, as well as for a Maxwellian evdf ($\kappa \rightarrow +\infty$) for direct comparison and validation. The mutual impedance response is computed for different plasma conditions characterized by the (equivalent Maxwellian) Debye length of the hottest electron population (from 30 cm to 5 m, renormalized by the corresponding Maxwellian evdf). The results are shown in **Figure 6**.

First, in the limit of the Debye, length is much smaller than the transmitter-receiver distance, the mutual impedance spectra are similar whatever the presence of suprathermal electrons (top left and right panels, corresponding to $\lambda_{D,Maxw}$ = 30 cm and $\lambda_{D,Maxw}$ = 1 m). In this regime, the mutual impedance measurement principle is therefore transparent to the presence and nature of suprathermal electrons and robust in determining the total electron plasma density.

Second, when the Debye length is slightly smaller, the mutual impedance spectra is flatter for high κ-values or a Maxwellian evdf than for low κ-values (bottom left and right panels, corresponding to $\lambda_{D,Maxw}$ = 2 m and $\lambda_{D,Maxw}$ = 5 m). Moreover, the maximum of the amplitude is shifted compared to the total electron plasma frequency for high κ-values or a Maxwellian evdf. In this regime, the presence of suprathermal electrons enables to detect the total plasma frequency on the mutual impedance spectra. This counter-intuitive result must be balanced by the fact that the mutual impedance spectra is computed for a smaller Debye length when the κ-value decreases. The comparison needs to be performed in the same plasma i.e., same electron density and electron temperature. Note that the

FIGURE 6 | Modeled PWI/AM^{2}P mutual impedance spectra for different $\lambda_{D,Maxw}$ (from 30 cm to 5 m) in a plasma modeled by a kappa evdf (κ = 2, 7, 24) and a Maxwellian evdf ($\kappa \rightarrow +\infty$). The amplitude is expressed in $20log_{10}$ and the frequency is normalized by the electron plasma frequency.

shape of mutual impedance response of a Maxwellian for $\lambda_{D,Maxw}$ = 2 m is similar to the response for a kappa evdf for $\lambda_{D,Maxw}$ = 5 m. Therefore, it is not possible to characterize the suprathermal electrons from the AM^{2}P spectra.

4.2.2. AM^{2}P Spectra With a Mix of a Halo Kappa and a Core Maxwellian evdf

To go beyond, we consider a plasma with a mix of a halo kappa and a core Maxwellian evdf, as observed in the solar wind by Pierrard et al. (2016). The AM^{2}P spectra have been computed in a large range of plasma parameters: the core-to-total density ratio n_c/n_{tot} varies from 0.1 to 0.9 and the halo-to-core temperature ratio T_h/T_c varies from 10 to 500 with the same Debye length $\lambda_{D,Maxw}$ = 4 m. This is reported in **Figure 7**, where the halo-to-core temperature ratio increases from left to right, while the density of the core electrons increases from bottom to top.

First of all, when the density of the core population is much higher that one of the halo (top panels), the mutual impedance spectrum is close to what is observed in a plasma modeled by a single evdf (**Figure 3**, top panels). Only one resonance appears close to the *total* electron frequency. In this limit, the response is independent to the κ-values of the halo evdf.

Second, when the plasma contains as many core electrons as halo electrons (middle row) or when the electron density is dominated by the halo part (third row), the shape of the mutual impedance spectra depends on the κ-value. As seen in the previous section, the resonance at the total plasma frequency is flatter when the kappa evdf tends to the Maxwellian evdf. With the Debye length considered here, the total electron density can be estimated for all κ-values. When the halo-to-core temperature ratio increases, a second resonance appears close to the core plasma frequency (blue vertical dotted line). This resonance is more pronounced when the halo-to-core temperature ratio increases whatever the κ- value. At a given halo-to-core temperature the amplitude of the electron acoustic mode increases with κ-value. This could be explained by the
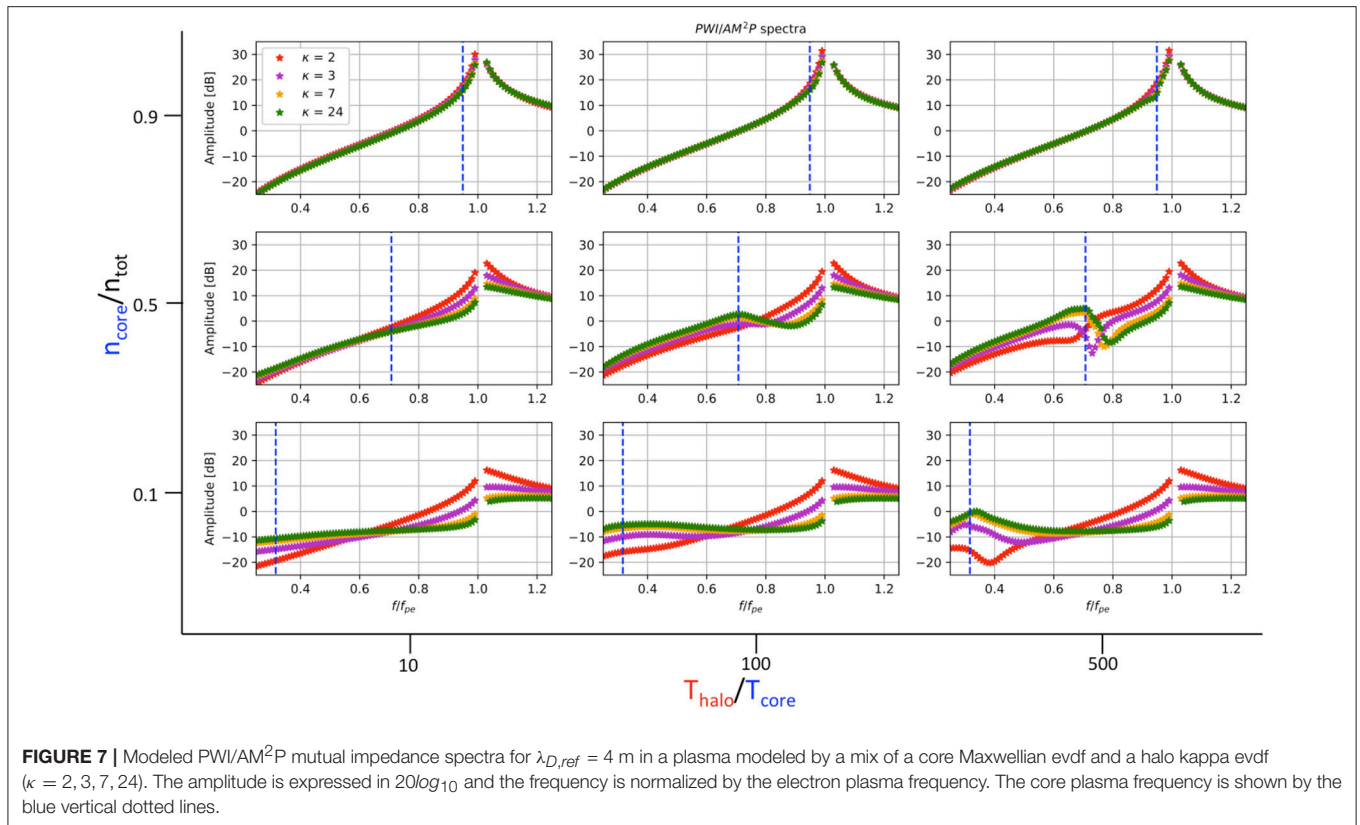
decay of the electron-acoustic mode domain of existence, with a fixed halo-to-core temperature ratio, in a presence of a mix of kappa and a Maxwellian evdf when the suprathermal electron part increases (Mace et al., 1999).

5. DISCUSSION

In the previous section, the mutual impedance spectra was modeled in a large domain of plasma parameters to characterize the effect of suprathermal electrons in the mutual impedance measurement. In this section, the AM^{2}P spectra is computed in the plasma conditions expected to be encountered by the MIO/MMO spacecraft: in the Hermean magnetospheric plasma (section 5.1) and in solar wind plasma close to the perihelion and the aphelion of Mercury (section 5.2). For that, we used the evdf found by fitting method with *in-situ* evdf measurement of the solar wind plasma (Maksimovic et al., 1997; Pierrard et al., 2016) and the energetic particle measurement of Mariner 10 during a flyby in the Hermean magnetospheric plasma (Baker et al., 1986).

5.1. AM^{2}P Spectra in the Hermean Magnetosphere

A large part of the elliptical orbit of MIO/MMO will be in the Hermean magnetosphere. In order to characterize the effect of the magnetospheric plasma in the AM^{2}P spectra, we used the observations of the electron density and the electron temperature measured by Mariner 10 during a flyby in the Mercury magnetospheric plasma in the nightside of Mercury with the closest approach at 700 km of the surface. These measurements are summarized in Baker et al. (1986). The modeling of the mutual impedance response in the electrostatic limit is valid due to the fact that the cyclotron frequency was negligible (around 3 kHz) compared to the total plasma frequency (around 20 kHz). Different electron populations should be observed in the Hermean magnetosphere especially: (i) an electron population from the solar wind origin (n_{SW} from 7 to 12 cm^{-3}, T_{SW} from 22

FIGURE 7 | Modeled PWI/AM^{2}P mutual impedance spectra for $\lambda_{D,ref}$ = 4 m in a plasma modeled by a mix of a core Maxwellian evdf and a halo kappa evdf (κ = 2, 3, 7, 24). The amplitude is expressed in $20log_{10}$ and the frequency is normalized by the electron plasma frequency. The core plasma frequency is shown by the blue vertical dotted lines.

to 40 eV) and (ii) an electron population from the magnetosheath (n_{MAG} from 3 to 7 cm^{-3}, T_{MAG} from 12 to 40 eV). A mixed of the two populations can be observed in the magnetospheric plasma. We choose to model the two electron populations both by a Maxwellian evdf. The Debye length of the solar wind electron population is characterized by (resp. magnetosheath) 10.0 m $<$ $\lambda_{D,SW}$ $<$ 17.7 m (resp. 9.7 m $<$ $\lambda_{D,MAG}$ $<$ 27.0 m). Several examples of the modeled AM^{2}P spectra with different configuration of the mix of the two electron populations are shown in **Figure 8**. For the considering cases, the resonance above the total electron plasma frequency is particularly flat, due to the large Debye length of the two electron populations compared to the transmitter-receiver distance. Therefore, the detection of the total electron plasma frequency, and therefore the measurement of the electron density will be challenging in the Hermean magnetosphere. Moreover, the resonance close to the plasma frequency corresponding to the electrons from the magnetosheath is not visible due to the fact that the temperature ratio is too low (see **Figure 7**). Therefore, the presence of two electron populations might not be observed by AM^{2}P in this regime of parameters.
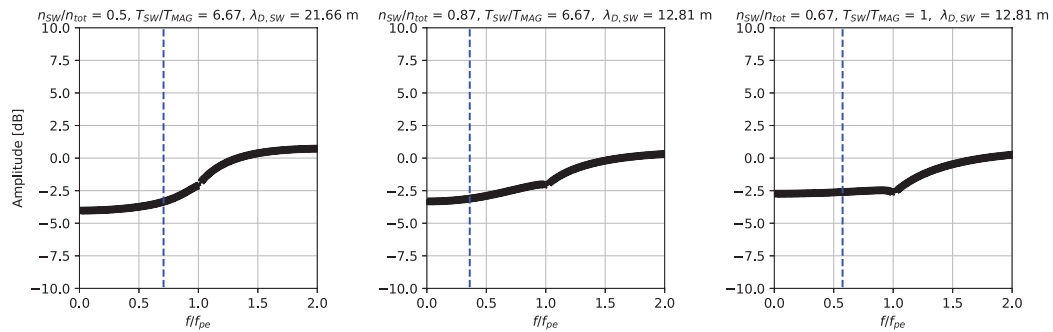
5.2. AM^{2}P Spectra in the Solar Wind Plasma Close to the Perihelion and Aphelion of Mercury

Mercury has the largest planetary orbital eccentricity in the Solar system. The distance to the Sun varies from 0.31 AU at perihelion

to 0.47 AU at aphelion. We modeled the AM^{2}P spectra in the solar wind plasma for both heliocentric distance.

First, close to the perihelion at 0.35 AU, the evdf of the solar wind has been characterized by a mix of a halo kappa evdf and a Maxwellian core evdf with a halo-to-core density ratio n_{halo}/n_{core} equals to 0.03 (n_{core}/n_{tot} = 0.97) and a halo-to-core temperature ratio T_{halo}/T_{core} equals to 3.36 with κ_h = 7.54 (Pierrard et al., 2016). The Debye length of the core population (resp. halo) is $\lambda_{D,core}$ = 3.73 m (resp. $\lambda_{\kappa,halo}$ = 33.4 m). The corresponding mutual impedance spectra in the solar wind at 0.35 AU is shown in **Figure 9** (red line, right panel). In order to characterize the effect of the suprathermal electrons in the solar wind in the AM^{2}P spectra, the AM^{2}P spectra has been modeled with only the core Maxwellian evdf (blue dotted line, right panel). We observed that the AM^{2}P spectra modeled by a sum of a core Maxwellian and a halo kappa evdf (red curve) and only with the core Maxwellian (blue curve) are similar. Also, the AM^{2}P spectra is flat (large resonance spectral signature) with a spectral peak (Ω = 1.25) shifted with respect to the plasma frequency (Ω = 1), while the cut-off frequency enables to retrieve efficiently the plasma frequency. Therefore, close to the perihelion of Mercury, the AM^{2}P experiment is robust to the presence of suprathermal electrons, seen as the halo part of the evdf, in the solar wind when determining the total electron density.

Second, the AM^{2}P spectra has been modeled in the solar wind plasma at 0.5 AU, close to the aphelion of Mercury (0.47 AU). The halo-to-core density ratio n_{halo}/n_{core} is equals to 0.04, the halo-to-core temperature T_{halo}/T_{core} is equals to 4.10 and κ_h =

FIGURE 8 | Modeled AM^{2}P spectra in three different plasma with a mix of electrons from the solar wind origin and the electrons from the magnetosheath, both modeled by a Maxwellian evdf. The amplitude is expressed in $20log_{10}$ and the frequency is normalized by the electron plasma frequency. The core plasma frequency is shown by the blue vertical dotted lines.
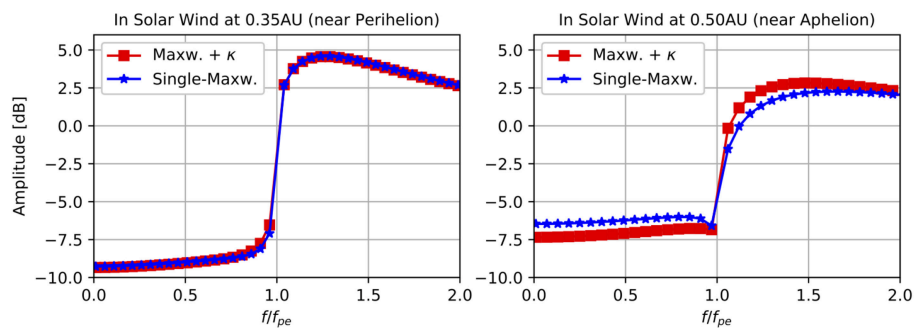
FIGURE 9 | Modeled PWI/AM^{2}P mutual impedance spectra for (i) a core Maxwellian evdf and a halo kappa evdf (red squared line) and (ii) only the core Maxwellian evdf (blue asterisk line) in the *in-situ* measured solar wind plasma at 0.35 AU (near Mercury perihelion, left panel) and 0.5 AU (near Mercury aphelion, right panel). The amplitude is expressed in $20log_{10}$ and the frequency is normalized by the total electron plasma frequency.

6.89 with $\lambda_{D,halo}$ = 46.37 m, $\lambda_{D,core}$ = 5.24 m (Pierrard et al., 2016). The modeled spectra is shown in **Figure 9** (right panel). Compared to the AM^{2}P spectra close to the perihelion (left panel), the AM^{2}P spectra at 0.5 AU is flatter. The maximum of amplitude is around 3 dB. This maximum is located far from the plasma frequency (Ω = 1.5) but the plasma frequency can be retrieved by the cut-off frequency. Due to the instrumental noise, we expect that the signal shall be measurable, with a low signal-to-noise ratio. Contrarily to the plasma conditions in the solar wind near perihelion, the shape of the spectra is affected by the suprathermal electrons modeled by a halo kappa evdf. Indeed, the spectra corresponding to the single-Maxwellian core (blue asterisk line) is different to the spectra modeled by the mix of the core Maxwellian and the halo kappa. However, the shape is closely similar which do not enable to separate the two electron populations and therefore it do not provided a measurement of the suprathermal electrons.

In this study, we have assumed that the solar wind strahl can be neglected. At the location of the perihelion (0.31 AU) and the aphelion (0.45 AU) of Mercury, the strahl contribution represents around 2–3% of the total electron density, less than the halo that represents from 8 to 10% (Maksimovic et al., 2005). Also the

"equivalent" strahl temperature would be higher than the halo one. Since in similar conditions expected to be encountered by BepiColombo, the halo contribution to the mutual impedance spectra is found to be negligible close to the perihelion, therefore, we expect the strahl contribution to the mutual impedance spectra to be even less significant than the halo part itself. However, the halo evdf can modify the shape of the spectra close to the aphelion. Therefore, if the strahl might slightly and marginally affect the mutual impedance spectra, we expect it to be within 1dB which is hardly detectable experimentally.

6. CONCLUSION

Mutual impedance experiments strongly depend of the electron velocity distribution function (evdf) encountered in the *in-situ* observed space plasma. This study illustrates the influence of suprathermal electrons on the instrumental response of mutual impedance experiments in the interplanetary plasma where the Debye length is of the order of the transmitter-receiver distance. Suprathermal electrons are observed in the Solar system as in the solar wind (Maksimovic et al., 1997), in the ionosphere of the comet 67P/Churyumov-Gerasimenko (Clark et al., 2015; Broiles

et al., 2016; Myllys et al., private communication) and in the Hermean magnetosphere (Christon, 1987). These electrons are usually modeled by (i) a kappa (Maksimovic et al., 1997) or a mix of core Maxwellian evdf and a halo kappa evdf (Pierrard et al., 2016). Thus, we have modeled the longitudinal dielectric function and the electrostatic radiated potential in a plasma modeled by these two different evdf, using and extending the numerical method developed in Gilet et al. (2017). We apply the modeling in the case of the mutual impedance experiments PWI/AM^{2}P onboard the MIO/MMO spacecraft of the BepiColombo mission, successfully launched in October 2018. First, we show that for a single evdf such as a kappa evdf, the radiated potential is more damped and the wavelength is smaller with the presence of suprathermal electrons. For the same electron temperature, the (Langmuir) resonance close to the electron plasma frequency is more visible on mutual impedance spectra than for a Maxwellian evdf when the Debye length increases and is of the order of the transmitter-receiver distance. When the plasma is modeled by a core Maxwellian evdf and a halo kappa evdf, as for a sum of two maxellian evdf (Gilet et al., 2017), an other resonance appears before the total plasma frequency due to the existence of the electron acoustic mode in a certain domain of the core-to-halo density and temperature. When the halo evdf is modeled by a kappa evdf with a low κ-value, the resonance due to the electron acoustic mode is less visible on the mutual impedance spectra. Second, we apply the modeling in a more realistic plasma in order to characterize the robustness of the experiment in the Hermean magnetospheric and the solar wind plasma. We show that the halo component of the evdf typically observed in the solar wind is neglected by the AM^{2}P experiment close the perihelion but it can slightly affect the spectra close to the aphelion. Moreover, the AM^{2}P experiment operating in Double-Wire (push-pull) mode should be in the limit of the measurement of the electron density when operating in the low density Hermean magnetospheric plasma. We expect the mutual impedance spectra acquired in these regions to be rather flat so that the expected resonance close to the plasma frequency might not be clearly visible in the low-density plasma surrounding Mercury. Therefore, the detection of the plasma frequency might be challenging for the AM^{2}P experiment in such regions. Measurements of the plasma bulk properties from SORBET and the Langmuir Probes might cover the range of the electron density measurements in these regions. Note that the quasi-thermal noise spectroscopy is also

sensitive to the presence of suprathermal electrons modeled by a kappa evdf (Le Chat et al., 2009). In the contrary, this study shows that mutual impedance spectra acquired in the solar wind close to Mercury where MIO/MMO shall spend most of the operating time (either the free solar wind, the magnetosheath, or the mixing layer between the solar wind and the Hermean plasmas) will give access to the plasma density. In particular, the modeling of the AM2P mutual impedance spectra described in this paper shows that, in the solar wind plasma, the mutual impedance cut-off frequency will represent a fast and efficient estimation of the plasma frequency, and therefore of the plasma density, which represent direct useful practical input for the future data processing of the AM^{2}P instrument. This work should be used also in the future, for the mutual impedance experiment RPWI/MIME onboard the JUICE spacecraft. This experiment will operate in the Jovian system in order to constrain the plasma bulk properties in the Jupiter magnetosphere and in particular in the ionosphere of Ganymede.

AUTHOR CONTRIBUTIONS

NG: performed the analysis and wrote the paper; PH: Ph.D. supervisor, Lead Co-Investigator of AM2P, supervised the paper; GW: helped about the modeling of the mutual impedance response; MM: helped about the suprathermal electrons; OR: helped about the plasma physics; CB: helped about the background of the story of the mutual impedance experiment; J-LR: Principal Investigator of the RPWI/MIME experiment onboard JUICE, helped about the principle of the experiment.

ACKNOWLEDGMENTS

REFERENCES

Baker, D. N., Simpson, J. A., and Eraker, J. H. (1986). A model of impulsive acceleration and transport of energetic particles in Mercury's magnetosphere. *J. Geophys. Res.* 91, 8742–8748. doi: 10.1029/JA091iA08p08742

Baluku, T. K., Hellberg, M. A., and Mace, R. L. (2011). Electron acoustic waves in double-kappa plasmas: application to Saturn's magnetosphere. *J. Geophys. Res. (Space Phys.)* 116:A04227. doi: 10.1029/2010JA016112

Beghin, C. (1995). Series expansion of electrostatic potential radiated by a point source in isotropic Maxwellian plasma. *Radio Sci.* 30, 307–322. doi: 10.1029/94RS03167

Beghin, C., and Debrie, R. (1972). Characteristics of the electric field far from and close to a radiating antenna around the lower hybrid

resonance in the ionospheric plasma. *J. Plasma Phys.* 8, 287–310. doi: 10.1017/S0022377800007157

Beghin, C., Debrie, R., Berthelier, J. J., Roux, D., Galperin, I. I., Gladyshev, V. A., et al. (1982). High resolution thermal plasma measurements aboard the Aureol 3 spacecraft. *Adv. Space Res.* 2, 61–66. doi: 10.1016/0273-1177(82)90150-8

Béghin, C., Hamelin, M., Lebreton, J. P., Vallieres, X., Moré, J., and Henri, P. (2017). Electron temperature anisotropy associated to field-aligned currents in the earth's magnetosphere inferred from rosetta mip-rpc observations during 2009 flyby. *J. Geophys. Res.* 122, 6964–6977. doi: 10.1002/2017JA024096

Benkhoff, J., van Casteren, J., Hayakawa, H., Fujimoto, M., Laakso, H., Novara, M., et al. (2010). BepiColombo: comprehensive exploration of Mercury: mission overview and science goals. *Planet. Space Sci.* 58, 2–20. doi: 10.1016/j.pss.2009.09.020

Blomberg, L. G., Matsumoto, H., Bougeret, J.-L., Kojima, H., Yagitani, S., Cumnock, J. A., et al. (2006). MEFISTO An electric field instrument for BepiColombo/MMO. *Adv. Space Res.* 38, 672–679. doi: 10.1016/j.asr.2005.05.032

Broiles, T. W., Livadiotis, G., Burch, J. L., Chae, K., Clark, G., Cravens, T. E., et al. (2016). Characterizing cometary electrons with kappa distributions. *J. Geophys. Res.* 121, 7407–7422. doi: 10.1002/2016JA022972

Chasseriaux, J. M., Debrie, R. D., and Renard, C. R. (1972). Electron density and temperature measurements in the lower ionosphere as deduced from the warm plasma theory of the h.f. Quadrupole probe †. *J. Plasma Phys.* 8, 231–253. doi: 10.1017/S0022377800007108

Chateau, Y. F., and Meyer-Vernet, N. (1991). Electrostatic noise in non-Maxwellian plasmas - Generic properties and 'kappa' distributions. *J. Geophys. Res.* 96, 5825–5836. doi: 10.1029/90JA02565

Christon, S. (1987). A comparison of the mercury and earth magnetospheres: electron measurements and substorm time scales. *Icarus* 71, 448–471. doi: 10.1016/0019-1035(87)90040-6

Clark, G., Broiles, T. W., Burch, J. L., Collinson, G. A., Cravens, T., Frahm, R. A., et al. (2015). Suprathermal electron environment of comet 67P/Churyumov-Gerasimenko: observations from the Rosetta Ion and Electron Sensor. *Astron. Astrophysi.* 583:A24. doi: 10.1051/0004-6361/201526351

Décréau, P. M. E., Beghin, C., and Parrot, M. (1978). Electron density and temperature, as measured by the mutual impedance experiment on board GEOS-1. *Space Sci. Rev.* 22, 581–595. doi: 10.1007/978-94-009-9527-7_18

Fried, B. D., and Conte, S. D. (1961). *The Plasma Dispersion Function*. New York, NY: Academic Press.

Gilet, N., Henri, P., Wattieaux, G., Cilibrasi, M., and Béghin, C. (2017). Electrostatic potential radiated by a pulsating charge in a two-electron temperature plasma. *Radio Sci.* 52, 1432–1448. doi: 10.1002/2017RS006294

Grard, R. (1969). Coupling between two electric aerials in a warm plasma. *Alta Freq.* 38, 97–101.

Grard, R. (1997). Influence of suprathermal electrons upon the transfer impedance of a quadrupolar probe in a plasma. *Radio Sci.* 32, 1091–1100. doi: 10.1029/97RS00254

Henri, P., Vallières, X., Hajra, R., Goetz, C., Richter, I., Glassmeier, K.-H., et al. (2017). Diamagnetic region(s): structure of the unmagnetized plasma around Comet 67P/CG. *Month. Notices R. Astron. Soc.* 469, S372–S379. doi: 10.1093/mnras/stx1540

Ho, G. C., Starr, R. D., Krimigis, S. M., Vandegriff, J. D., Baker, D. N., Gold, R. E., et al. (2016). Messenger observations of suprathermal electrons in mercury's magnetosphere. *Geophys. Res. Lett.* 43, 550–555. doi: 10.1002/2015GL066850

Johnson, C. L., Purucker, M. E., Korth, H., Anderson, B. J., Winslow, R. M., Al Asad, M. M. H., et al. (2012). MESSENGER observations of Mercury's magnetic field structure. *J. Geophys. Res.* 117. doi: 10.1029/2012JE004217

Kasaba, Y., Bougeret, J.-L., Blomberg, L. G., Kojima, H., Yagitani, S., Moncuquet, M., et al. (2010). The Plasma Wave Investigation (PWI) onboard the BepiColombo/MMO: first measurement of electric fields, electromagnetic waves, and radio waves around Mercury. *Planet. Space Sci.* 58, 238–278. doi: 10.1016/j.pss.2008.07.017

Krall, N. A., and Trivelpiece, A. W. (1973). *Principles of Plasma Physics*. New York, NY: McGraw-Hill Book Company.

Lazar, M., Pierrard, V., Shaaban, S. M., Fichtner, H., and Poedts, S. (2017). Dual Maxwellian-Kappa modeling of the solar wind electrons: new clues on the temperature of Kappa populations. *Astron. Astrophys.* 602:A44. doi: 10.1051/0004-6361/201630194

Le Chat, G., Issautier, K., Meyer-Vernet, N., Zouganelis, I., Maksimovic, M., and Moncuquet, M. (2009). Quasi-thermal noise in space plasma: "kappa" distributions. *Phys. Plasmas* 16:102903. doi: 10.1063/1.3243495

Mace, R. L., Amery, G., and Hellberg, M. A. (1999). The electron-acoustic mode in a plasma with hot suprathermal and cool Maxwellian electrons. *Phys. Plasmas* 6, 44–49. doi: 10.1063/1.873256

Mace, R. L., and Hellberg, M. A. (1995). A dispersion function for plasmas containing superthermal particles. *Phys. Plasmas* 2, 2098–2109. doi: 10.1063/1.871296

Maksimovic, M., Pierrard, V., and Riley, P. (1997). Ulysses electron distributions fitted with kappa functions. *Geophys. Res. Lett.* 24, 1151–1154. doi: 10.1029/97GL00992

Maksimovic, M., Zouganelis, I., Chaufray, J.-Y., Issautier, K., Scime, E. E., Littleton, J. E., et al. (2005). Radial evolution of the electron distribution functions in the fast solar wind between 0.3 and 1.5 AU. *J. Geophys. Res.* 110:A09104. doi: 10.1029/2005JA011119

Meyer-Vernet, N., Issautier, K., and Moncuquet, M. (2017). Quasi-thermal noise spectroscopy: the art and the practice. *J. Geophys. Res.* 122, 7925–7945. doi: 10.1002/2017JA024449

Moncuquet, M., Matsumoto, H., Bougeret, J.-L., Blomberg, L. G., Issautier, K., Kasaba, Y., et al. (2006). The radio waves and thermal electrostatic noise spectroscopy (SORBET) experiment on BEPICOLOMBO/MMO/PWI: scientific objectives and performance. *Adv. Space Res.* 38, 680–685. doi: 10.1016/j.asr.2006.01.020

Navet, M., Bertrand, P., Feix, M., Rooy, B., and Storey, L. (1971). Problemes et modeles en theorie des sondes radiofrequences. *J. Phys. Colloq.* 32, C5b–189–C5b–191.

Pierrard, V., Lazar, M., Poedts, S., Štverák, Š., Maksimovic, M., and Trávníček, P. M. (2016). The electron temperature and anisotropy in the solar wind. Comparison of the core and halo populations. *Solar Phys.* 291, 2165–2179. doi: 10.1007/s11207-016-0961-7

Pottelette, R., Rooy, B., and Fiala, V. (1975). Theory of the mutual impedance of two small dipoles in a warm isotropic plasma. *J. Plasma Phys.* 14, 209–243. doi: 10.1017/S0022377800009533

Pottelette, R., and Storey, L. R. O. (1981). Active and passive methods for the study of non-equilibrium plasmas using electrostatic waves. *J. Plasma Phys.* 25, 323–350. doi: 10.1017/S0022377800023151

Rooy, B., Feix, M. R., and Storey, L. R. O. (1972). Theory of a quadripolar probe for a hot isotropic plasma. *Plasma Phys.* 14, 275–300. doi: 10.1088/0032-1028/14/3/005

Schippers, P., Blanc, M., André, N., Dandouras, I., Lewis, G. R., Gilbert, L. K., et al. (2008). Multi-instrument analysis of electron populations in Saturn's magnetosphere. *J. Geophys. Res.* 113:A07208. doi: 10.1029/2008JA013098

Schlumberger, C. (1920). *Étude sur la Prospection électrique du Sous-sol, par C. Schlumberger*, Paris: Gauthier-Villars.

Storey, L. R. O., Aubry, M. P., and Meyer, P. (1969). "A quadripole probe for the study of ionospheric plasma resonances," in *Plasma Waves in Space and in the Laboratory*, eds J. O. Thomas and B. J. Landmark (New York, NY: Edinburgh University Press), 303.

Štverák, Š., Maksimovic, M., Trávníček, P. M., Marsch, E., Fazakerley, A. N., and Scime, E. E. (2009). Radial evolution of nonthermal electron populations in the low-latitude solar wind: helios, Cluster, and Ulysses Observations. *J. Geophys. Res.* 114:A05104. doi: 10.1029/2008JA013883

Summers, D., and Thorne, R. M. (1991). The modified plasma dispersion function. *Phys. Fluids B* 3, 1835–1847. doi: 10.1063/1.859653

Trotignon, J. G., Béghin, C., Lagoutte, D., Michau, J. L., Matsumoto, H., Kojima, H., et al. (2006). Active measurement of the thermal electron density and temperature on the Mercury Magnetospheric Orbiter of the BepiColombo mission. *Adv. Space Res.* 38, 686–692. doi: 10.1016/j.asr.2006.03.031

Trotignon, J. G., Michau, J. L., Lagoutte, D., Chabassière, M., Chalumeau, G., Colin, F., et al. (2007). RPC-MIP: the mutual impedance probe of the Rosetta plasma consortium. *Space Sci. Rev.* 128, 713–728. doi: 10.1007/s11214-006-9005-1

Vasyliunas, V. M. (1968). A survey of low-energy electrons in the evening sector of the magnetosphere with OGO 1 and OGO 3. *J. Geophys. Res.* 73, 2839–2884. doi: 10.1029/JA073i009p02839

Wenner, F. (1915). A method for measuring earth resistivity. *J. Washington Acad. Sci.* 5, 561–563. doi: 10.1016/S0016-0032(15)90298-3